Measurement and Prediction of Energy Transfer Efficiency in Laser Beam Welding

A dimensionless parameter model is developed to estimate the laser energy absorbed by the workpiece

BY P. W. FUERSCHBACH

ABSTRACT. The absorption of laser energy by the workpiece during laserbeam welding (LBW) has been studied through direct measurements of heat input obtained with a Seebeck envelope calorimeter. The experiment compared workpiece materials with contrasting thermal properties (304 stainless steel, 1018 steel, tin), and varied the laser power, travel speed, and focus spot size in order to determine their effects on two figures of merit: the energy transfer efficiency and the melting efficiency. An uncertainty analysis of the experimental measurements and calculated parameters has been included.

The energy transfer efficiency during laser beam welding was found to increase with beam intensity from 0.20 to 0.90 and to stabilize at a high value at intensities greater than 30 kW/cm. No correlation with energy transfer efficiency was found for either the fusion zone depth-to-width ratio or the travel speed. Measured melting efficiencies for laser welding were found to be no higher than the theoretical maximum value of 0.48 which can be obtained with conventional arc welding processes. However, improved melting efficiency over conventional processes was obtained due to the shapes of laser welds that create two-dimensional heat flow in nominally three-dimensional heat flow applications.

A mathematical model for laser welding has been developed using dimensionless parameters that relate the size of a laser weld to the net heat absorbed by the workpiece. Through application of this model, the energy transfer efficiency for continuous wave laser welding processes can be calculated after measurements of weld cross-sectional area have been made. Use of this model is expected to assist in optimization of laser welding for any type of material when it is used to select processing regimes that maximize melting efficiency and energy transfer efficiency.

P. W. FUERSCHBACH is with the Physical and Joining Metallurgy Dept. at Sandia National Laboratories, Albuquerque, N.Mex.

Introduction

Laser beam welding (LBW) is often selected for critical manufacturing applications because a laser is considered to be an extremely precise heat source which can produce high-quality fusion welds with weld geometries that are unobtainable with conventional arc welding processes. But in one very important way, the LBW process is not as precise a process as arc welding. Though it is not widely considered as such, an important figure of merit for any welding process is the energy transfer efficiency[1]. The absorption of arc energy by the workpiece for welding processes like gas tungsten arc welding (GTAW), or gas metal arc welding (GMAW), is relatively invariant to manufacturing conditions such as power level or the location of the workpiece surface (Ref. 1). However, for LBW, it is soon evident to anyone working with the process that the absorption of laser beam energy by the weldment is strongly dependent on both the laser power and the positioning of the workpiece relative to the focused laser beam. One can see that in critical welding applications where melt-through could be catastrophic, it is preferable to use a process that cannot abruptly increase the energy transferred because of a slight change in workpiece positioning or power output.

Nevertheless, lasers have several valuable attributes for advanced manufacturing that cannot be overlooked, including a very small spot size, line-of-sight access to weld joints, and most importantly, deep joint penetration. As a result, LBW is widely used in critical joining applications but with process control procedures specifically developed to minimize the effects of variable beam absorption. There are two ways that have proven effective in preventing variable beam absorption: 1) strict process control procedures are developed which insure that neither the laser power nor the incident spot size can vary appreciably, or 2) a processing regime is found where the

KEY WORDS

Laser Beam Welding
Uncertainty Analysis
Intensity
Dimensional Analysis
Melting Efficiency
Microwelding
Irradiance
Calorimetry
CO_2 Laser
Absorption

1. For laser welding, energy transfer efficiency is defined as the ratio of the heat absorbed by the workpiece to the incident laser energy. It is a dimensionless parameter.

Table 1 —Thermophysical Properties of Materials Welded

Material	Liquidus Temperature	Thermal Diffusivity @ 300K	(mm^2/s) @ Liq. Temp.	Enthalpy of Melting (J/mm^3)
304 stainless steel	1727K	3.95 (Ref. 11)	5.7 (Ref. 12)	8.7 (Ref. 13)
1018 steel	1798K	16.5 (Ref. 11)	5.5 (Ref. 12)	10.4 (Ref. 14)
tin	505K	40.2 (Ref. 11)	17.3 (Ref. 11)	0.78 (Ref. 14)

energy transfer efficiency is relatively insensitive to fluctuations in power or focus spot size. The author has seen both practices used in manufacturing, though the underlying reasons for the success of the latter are not generally well understood.

The absorption of laser beam energy by the workpiece in LBW is a complex subject that has resulted in several theories about the mechanism responsible. It has been observed by several researchers that a dramatic increase in absorption of laser beam energy occurs above a critical level of laser beam irradiance (power per unit area) (Refs. 2–4). It is also known that this beam absorption significantly decreases at a still higher irradiance where laser supported plasmas are thought to attenuate the laser beam (Refs. 2, 3). Since the laser power level required to achieve a specific depth of penetration is directly dependent on the energy transfer efficiency achieved, there is strong interest in this research. Not surprisingly, many investigators have attempted to predict the energy transfer efficiency based on knowledge of the laser process parameters and the resulting weld dimensions (Refs. 2, 4–6). These predictions enable the ultimate potential of a particular laser design to be quantified and are a prerequisite for most computer models of the process.

Melting efficiency[2] is another figure of merit that has been widely speculated about for the LBW process, but has not been experimentally well validated. Since LBW has often proven to be effective in minimizing the heat input to the workpiece, the process has been thought to possess an intrinsically high melting efficiency (Refs. 7, 8). One expects that the extremely high irradiance of the process minimizes heat conduction into the base metal. Indeed, the selection of LBW for many welding applications is often made solely to ensure minimum heat input to the part. But this is a questionable assumption when one considers that no standard methodology exists for selecting process parameters to maximize LBW melting efficiency and low heat input LBW weld schedules must be determined empirically just as they are for arc welding applications. Clearly, the lack of understanding of LBW melting efficiency and energy transfer efficiency are interrelated, since an accurate determination of the net heat input to the workpiece is required to calculate either of these figures of merit.

This study is an extension of calorimetric measurements which have determined the energy transfer efficiency and the melting efficiency for pulsed and continuous power GTAW and plasma arc welding (PAW) (Ref. 9). Those measurements concluded that the theoretical maximum melting efficiency of 0.48 (Refs. 4, 10) could be achieved with an arc welding process if the process parameters meet certain criteria and the joint geometry promotes two-dimensional heat flow. In this study, calorimetric measurements of the continuous-power CO_2 LBW process have been made to determine the maximum melting efficiency of the process, to find what process parameters affect it, and to see if LBW has an advantage over arc welding in melting efficiency. In addition, since the energy transfer efficiency for LBW is known to have a strong dependence on the laser beam irradiance, the effect of laser beam power and focusing on the energy transfer efficiency have been investigated.

Experimental

Bead-on-plate-type partial penetration laser welds were made on three different materials in this study: 304 stainless steel (SS), 1018 low-carbon steel, and pure tin. The thermophysical properties of these materials are given in Table 1. The materials were chosen for this study because they all have significantly different room-temperature thermal diffusivities and were expected to display divergent welding behavior as was the case in an earlier study with 304 SS and pure nickel (Ref. 9). All three materials were cut from as-rolled plate into test specimens 12.7 x 50.8 x 102 mm (0.5 x 2 x 4 in.). The depth of weld penetration and the thickness of the plate were chosen in order to obtain three-dimensional heat flow conditions around the fusion zone (Ref. 15). The flat surfaces of the 304 SS and 1018 specimen plates were degreased and welded in the as-received condition. The pure tin specimens were lapped to a 32-μin. scratch-free finish to assure surface uniformity. Up to seven individual welds (depending on the resulting weld width) 89 mm (3.5 in.) long were made on the flat side of each specimen. The spacing between welds was adjusted to account for the preceding

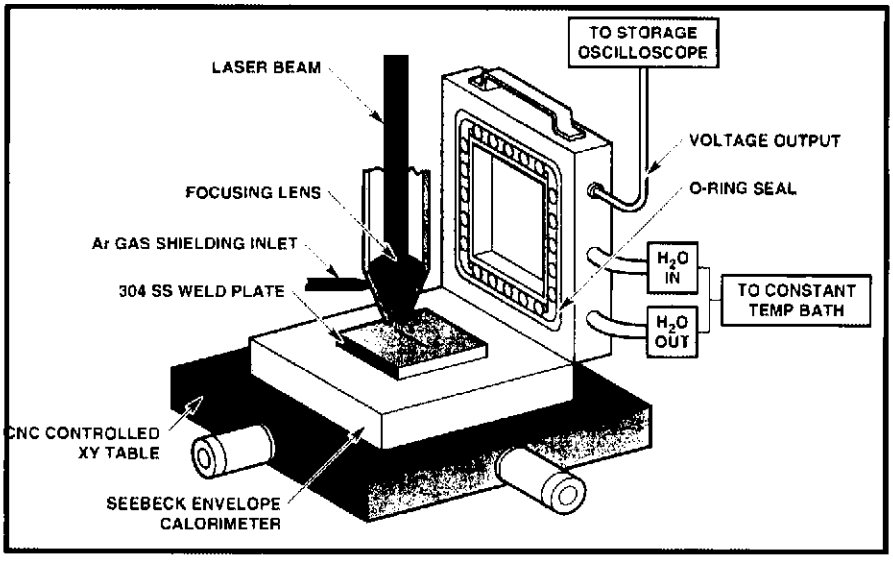

Fig. 1 — CO_2 laser beam welding calorimetric experimental set up.

2. Melting efficiency is defined as the ratio of the heat necessary to just melt the fusion zone to the heat absorbed by the workpiece. It is a dimensionless parameter.

weld's width. Most welds were made in a single pass but welds that resulted in a low heat input signal to the calorimeter were made in a non overlapping U-shaped double pass. All of the welds were made automatically by a CNC motion controller, which directed the gas shielding, the table motion, and the laser shutter.

The test specimens were mounted to the base plate of a Seebeck envelope calorimeter as shown in Fig. 1. The internal dimensions of the calorimeter are 150 x 150 x 75 mm (6 x 6 x 3 in.). The CNC-controlled X-Y table translated the calorimeter under the focused laser beam. The calorimeter was left open during welding and closed immediately after the weld was completed. The calorimeter walls are maintained at room temperature with a constant-temperature bath. The calorimeter operates on the gradient layer principle (Ref. 16) and produces a voltage output that is proportional to the flux through the walls during the time required for the weld sample to cool to room temperature. For short duration weld times, the energy losses with this experimental technique due to radiation, convection, and evaporation have been estimated to be 1% or less of the measured energy (Ref. 17). The calorimeter has been shown to produce a very linear response for different closure time duration's and heat input levels. It was calibrated for this study using a transient water heat content method as detailed earlier (Ref. 17).

Welds were made using a Photon Sources V1200 slow axial flow CO_2 laser operating in the continuous-wave mode. The welds were shielded with 100% argon gas from a nozzle assembly that also housed the focusing lens. The lenses were protected from weld spatter with a zinc-selenide cover glass. The zinc-selenide focusing lenses used in this experiment are listed in Table 2. Aspheric lenses were used for the short focal lengths to increase irradiance. The lenses were chosen in order to achieve a large range of irradiance for the materials welded. Also listed in Table 2 are the measured minimum spot diameters and the depth of focus for each lens used in the study (Ref. 18). These data were used in the determination of beam irradiance and intensity. The focus spot size was measured using the Prometec Laserscope UFF 100 laser beam diagnostic system, which uses a rotating hollow needle to map the unattenuated focused laser beam spatial power distribution, and a lap top personal computer to collect the data and calculate an effective spot size. The spot size as calculated by this system includes 86% of the total power in the beam. For each lens, measurements were made at several positions about the focal plane. The resulting data were curve fit to the laser beam propagation equation in order to determine the minimum spot size (Ref. 19).

Table 2 — Focusing Lens Characteristics

Lens Type	Nominal Focal Length	F number	Incident Angle (deg)	Focus Spot Diameter	Depth of Focus
Aspheric	2.5 in. (63.5 mm)	3.3	17.4	0.118 mm	0.29 mm
Aspheric	3.75 in. (95.2 mm)	4.9	11.7	0.164 mm	0.58 mm
Meniscus	5.0 in. (127 mm)	6.5	8.8	0.224 mm	1.18 mm
Plano Convex	7.5 in. (191 mm)	9.8	5.8	0.294 mm	2.25 mm

The laser beam was focused on the workpiece by making a series of welds where the lens-to-workpiece distance was varied in small, precise increments. Previous work by Brandon (Ref. 20) with this laser has indicated that for partial joint penetration welds, the weld with the greatest width on the surface for a given power and lens usually corresponds to the weld with the deepest penetration. This author has not found the effect to be as consistent with Nd:YAG lasers. Nonetheless, this approach has merit here and was used to expedite the determination of sharp focus for the many experimental conditions examined. The weld that appeared to have the greatest weld width was assumed to be in focus, and the corresponding lens position was selected for subsequent welds with that lens.

Laser output power was measured with an Optical Engineering Model 25-D power probe either immediately before each weld or immediately after completion of the weld. The power measurements were taken in the laser beam as it exited the focusing lens nozzle assembly. The CNC controller regulated the probe exposure time.

The output voltage of the calorimeter was recorded on a digital storage oscilloscope with a long duration trace from the start of the weld until the sample cooled down to the bath temperature. When the mass inside the calorimeter reaches the temperature of the water bath, the output voltage becomes zero. The output voltage vs. time trace was then integrated to determine the energy in joules absorbed by the workpiece during the weld (*i.e.*, the net heat input). The reported values of energy transfer efficiency (η_t) were calculated by dividing the net heat input (Q_i) by the laser output energy (Q_o), which is the output power multiplied by the shutter open time.

$$\eta_t = \frac{Q_i}{Q_o} \tag{1}$$

The enthalpy of the weld volume was determined by multiplying the fusion zone volume by the enthalpy change (δh) required to bring a unit volume of the metal from room temperature (T_r), to the liquidus temperature (T_l). It is given by the following expression and includes the heat of fusion (Δh_f), and the sensible heat:

$$\delta h = \Delta h_f + \int_{T_r}^{T_l} c_p(T)dT \tag{2}$$

Since the specific heat is a function of temperature, empirical not calculated values of δh were used and are given in Table 1.

Joint penetration was measured from the plate surface to the weld root of the fusion zone and was determined from the average of four metallographic cross-sections. Weld cross-sectional area was determined (using a planimeter) from the average of four transverse metallographic sections taken from each weld. These areas were multiplied by the weld length to determine the total fusion zone volume (V). The values of melting efficiency (η_m) were calculated by dividing the enthalpy of the weld volume by the net heat input as given by the following expression:

$$\eta_m = \frac{V\delta h}{Q_i} \tag{3}$$

The primary independent variables were laser output power and travel speed, which, besides material type, are the principal factors that affect melting efficiency. For the majority of welds made, these two factors were each varied at five levels in order to produce welds with a wide range of fusion zone size and heat input. It has been predicted (Ref. 21), and indeed is intuitive, that unusually high travel speed levels can lead to a drop in melting efficiency. To verify this decrease, two significantly high

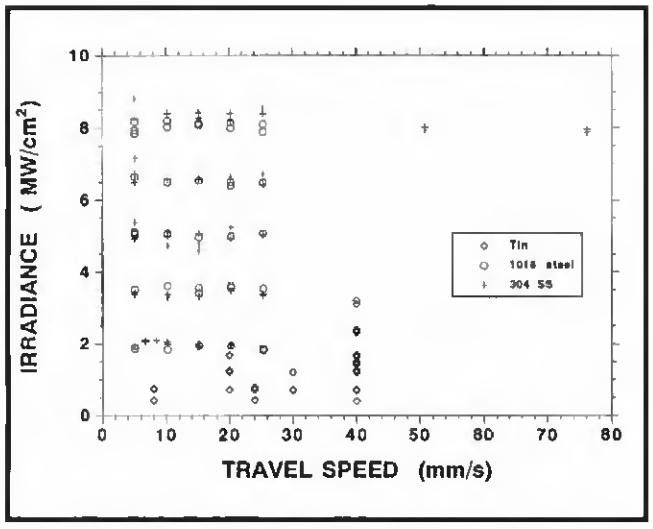

Fig. 2 — Range of travel speed and beam irradiance for three materials in the experiment, all conditions produced practical fusion welds.

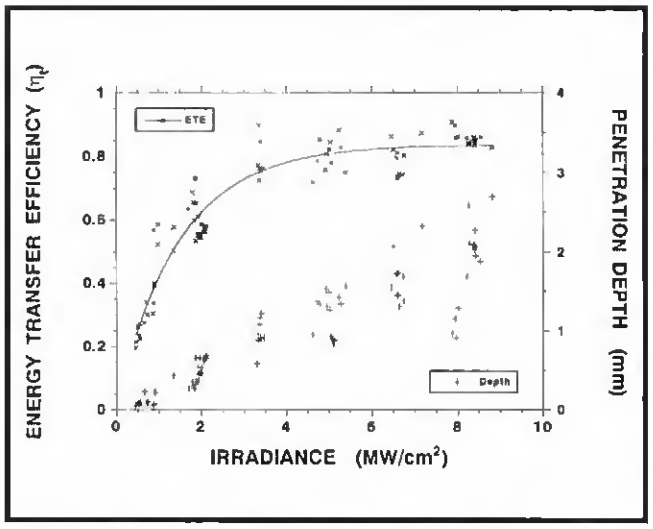

Fig. 3 — Variation of measured energy transfer efficiency and weld penetration with beam irradiance for 304 stainless steel.

travel speed levels were also tested for the 304 SS material.

All of the 304 SS and 1018 steel welds were made with the same 2.5-in. (63.5-mm) aspheric focusing lens, which produced a very small spot size and thereby provided sufficient irradiance to make welds at low laser power. For the tin, the irradiance required to make welds was significantly lower, and longer focal length lenses and higher travel speeds were used to vary the fusion zone size and to observe the effect of a third independent variable—the focus spot size. The spot size was varied for the tin welds by selecting different focal length lenses. The 2.5-in. aspheric lens was not used to weld tin because of excessive spatter. Each of the other three lenses listed in Table 2 were used to weld the tin.

A sample uncertainty analysis of the experimental measurements and derived parameters is given in the Appendix. It is based on the ANSI/ASME standard on measurement uncertainty (Ref. 22). The uncertainty analysis contains information about the relative importance of precision error or bias error for a nominal value of a reported parameter. In addition, the uncertainty analysis is valuable as it indicates the propagation of error from measured parameters into derived parameters.

Results and Discussion

Energy Transfer and Penetration

The range of travel speed and laser beam irradiance used for the three materials examined in this study can be seen in Fig. 2. Each of these conditions identifies a weld that could be examined on the workpiece surface, that was suitable for metallographic cross-sectional examination, and did not experience significant weld metal displacement (spatter) from the fusion zone. As a result, the values of irradiance shown in Fig. 2 represent a practical operating range for welding these materials with this laser. This figure however, does not likely cover the entire operating range for welding these materials, since higher irradiances could not be obtained with this laser. In any case, it is prudent not to extrapolate outside the boundaries of the experiment because excessive irradiance can easily lead to the onset of drilling.

The variation of energy transfer efficiency with laser beam irradiance for 304 SS is shown in Fig. 3. Also given on the second ordinate in the figure is the corresponding weld penetration for each irradiance value. The least squares curve fit through the irradiance data illustrates the increase in energy transfer which was seen to occur for all three of the materials tested. One can see that while the increase in absorption by the workpiece is dramatic, it is not an abrupt increase as some researchers have proposed (Ref. 23).

Another important observation one can make from Fig. 3 is that the energy transfer efficiency essentially reaches a constant value above an irradiance level of about 3 MW/cm^2. In addition, there is an extensive processing region (from 3 to 9 MW/cm^2) where the absorption of laser energy is at a maximum and relatively invariant. It is the authors contention that all laser welding should be conducted in this plateau region. Only in this region will the laser resonator output power be fully utilized. Perhaps more importantly, in this region the laser energy absorption by the part will be insensitive to part positioning errors that will often change the workpiece irradiance. One can conclude from Fig. 3 that to assure a consistent absorption of laser beam energy by the workpiece, a high laser beam irradiance is required. With many lasers, in order to operate in this plateau region, a very small spot size will be necessary. As a result, the somewhat common practice of defocusing the laser beam to increase the weld pool width will likely result in reduced process consistency.

It is clear from Fig. 3 that while the energy transfer efficiency reaches a plateau value, the weld joint penetration does not, but continually increases for each level of irradiance examined. The large variance in joint penetration seen for each level of irradiance is due to the multiple levels of travel speed represented — as one expects, the travel speed controls the local amount of energy available for melting. The causal relationship between weld joint penetration and beam irradiance is an important characteristic of LBW and electron beam welding that distinguishes them among other fusion welding processes. The increase in joint penetration with irradiance shown in Fig. 3 indicates that the depth of joint penetration is controlled by the depth of the laser supported vapor cavity (keyhole). This characteristic of LBW is a potential advantage in many applications. Unlike many arc welding processes where the penetration depth is controlled by composition-sensitive convective currents in the weld pool, LBW can make narrow and deep welds in materials that are difficult to penetrate with arcs. If laser weld pool shape depends on vaporization

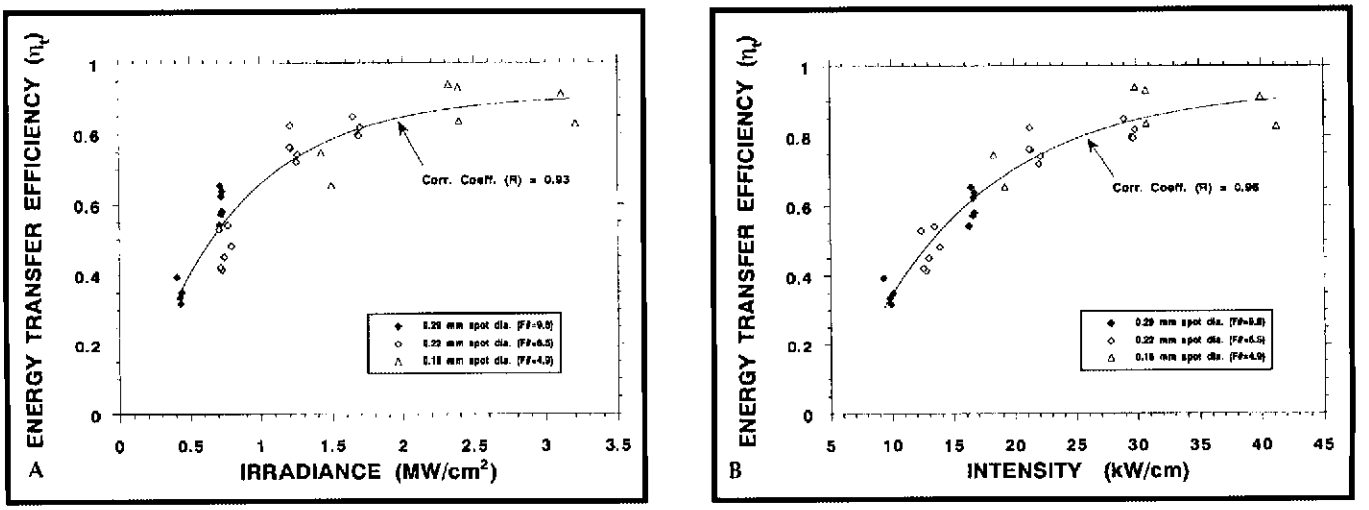

Fig. 4 — A — Effect of laser spot size on the correlation between measured absorption and beam irradiance for tin welds; B — correlation between measured absorption and laser beam intensity for tin welds with variable spot size.

rather than on convection, one can expect penetration to be less dependent on levels of surface active elements in the material with this process. In addition, this effect has important implications for predicting weld joint penetration, since one may be able to select the weld penetration *a priori* if the mathematical relationship between joint penetration, irradiance, and travel speed is known.

One can also see from Fig. 3 that the large changes in travel speed that significantly perturb weld penetration do not likewise affect the energy transfer efficiency. Essentially, the scatter shown about the fitted curve was not found to be consistent in any way with the changes in travel speed but is instead attributed to precision error (see Appendix) in the measurements of irradiance and energy transfer efficiency.

It is also apparent from the figure that high energy transfer efficiencies were achieved over a wide range of penetration depths. It has been reported (Refs. 24, 25) that in order to achieve good coupling of a laser beam with the workpiece, a keyhole-like cavity must be created where the laser beam is absorbed. The laser beam cannot be reflected out of this cavity but is instead captured by multiple internal reflections within. This absorption mechanism has been proposed since it is known that the absorption of infrared radiation by liquid metals is very low (Ref. 26). Arata has measured the absorption of CO_2 radiation for molten iron and 304 stainless steel to be less than 15% (Ref. 27). In order to account for a 90% energy transfer efficiency, the laser light must be absorbed on additional surfaces within the cavity.

For the keyhole absorption mechanism, one might expect the resulting cross-sectional shape of the fusion zone to indicate whether a weld had either high or low energy transfer efficiency. For the partial penetration welds of this study, the fusion zone aspect ratios were not a consistent indicator of energy transfer efficiency. Despite the fact that the highest fusion zone depth-to-width ratios logically coincided with the highest irradiances, and therefore, the highest energy transfer efficiencies, no significant correlation between fusion zone aspect ratio (depth/width) and energy transfer efficiency was found for the materials examined. In related work with aluminum, Mallory, *et al.* (Ref. 28), found that CO_2 laser beam absorption did not correlate with the depth of joint penetration. This inconsistency does not indicate that absorption is unrelated to the depth of weld penetration, but only that the resulting shape of the weld is driven by other more dominant factors such as heat conduction and convective flow, which could mask the connection to a keyhole geometry.

Unlike the 304 SS welds, the tin welds were not all made with the same focusing lens. Consequently, variation in laser beam irradiance was achieved not only by changing the output power, but also by changing the focus spot size. As one would expect, for a given power, the highest energy transfer efficiency was obtained with the smallest spot size. By normalizing the effect of power by the focal spot area as in Fig. 3, it is implied that the focal spot area is the only factor besides power that is important in energy transfer. However, for the tin welds, it was discovered that another factor is important. We will refer to the ratio of laser output power to the focused spot diameter as the laser intensity. The variation of energy transfer efficiency with laser beam irradiance and intensity for tin is illustrated in Fig. 4A and B, respectively. Close examination of Fig. 4A reveals that the energy transfer efficiency does not appear to be solely a function of the beam irradiance but is also affected by the focal length of the focusing lens. When laser power is divided by the laser spot diameter (Fig. 4B) rather than the spot area (Fig. 4A), a better curve fit is obtained. Similar results were obtained by Beyer, *et al.* (Ref. 29), who found that for welds of the same irradiance the deepest weld joint penetration was obtained for the lens that gave the largest spot size.

Since dividing output power by the spot diameter is equivalent to multiplying the irradiance by the spot diameter, one can presume there is some additional unaccounted for effect of a larger spot diameter. One potentially important additional effect of a larger spot size may be a change in the angle of incidence of the laser beam. Since the angle of beam incidence in radians is the inverse of the F number of the focusing lens, increasing the focal length of the lens significantly decreases the incident angle — Table 2. Absorption through constructive interference in a very thin liquid metal film at the walls of the keyhole could be a mechanism to explain a dependence on incident angle. In another paper (Ref. 30), Beyer, *et al.*, found that weld joint penetration was dependent on the polarization of the laser beam. Absorption of light by thin metallic films is well known to be dependent on the incident angle of the light and its degree of polarization.

The strong dependence of energy transfer efficiency on the magnitude of laser intensity shown in Fig. 4B for tin was found to be of a similar degree for the two Fe-based alloys examined. Figure 5

illustrates this dependence for all of the welds made in this study. As was the case for the 304 SS data alone, the variation in energy transfer efficiency about the fitted curve for the other two materials was not found to be due to changes in travel speed. One can see that although there is some scatter about the fitted curve, it is not clear if one material absorbs the incident beam more readily than another. It is difficult to infer from theory which material will have greater absorption since as pointed out by Mazumder (Ref. 31), calculation of absorption from the electrical resistivity will be valid only for metals heated in a vacuum. The rate of metal oxidation likely depends on the levels of the process parameters, as well as the effectiveness of the argon shielding. Therefore, one cannot know the degree of oxidation, or indeed predict if one material will have a higher absorption than another for a given laser intensity.

Melting Efficiency

As expected from the experimental design, the measured melting efficiencies for the LBW process varied widely and were found to be dependent on the same process parameters as in an earlier study of arc welding processes (Ref. 9). Figure 6 shows that the measured melting efficiencies for all three materials increase as the laser power is increased. The large fluctuation in melting efficiency for each material at a given output power is due to the variation in the other process parameter: travel speed. One can see from the figure that as power is increased, the melting efficiency asymptotically approaches a maximum value. It is interesting to note that the highest values of melting efficiency measured in these experiments were very close in magnitude to the theoretical maximum of 0.48 for two-dimensional heat flow first given by Rykalin (Ref. 10). This close agreement to theory serves to corroborate the validity of the experimental technique used in this study. It is also apparent from Fig. 6 that high melting efficiency can be obtained at relatively low laser output powers and without pulsing of the laser power. It has been stated in the welding literature (Ref. 32) that pulsed lasers, because of their high peak power, are required for efficient laser welding. This is clearly not the case, since energy transfer efficiencies and melting efficiencies close to the theoretical maximums have been obtained in this study with continuous power as low as 500 W. This situation is directly analogous to the effect of pulsed current on melting efficiency in GTA welding as detailed by Fuerschbach and Knorovsky (Ref. 9), where at low travel speeds, pulsed power does in fact increase the melting efficiency over continuous power; however, at high travel speeds there is no difference between the two power modes since melting efficiency is already close to the theoretical maximum and can rise no further.

The important effect of travel speed on melting efficiency for the three materials is illustrated in Fig. 7. One can see again, as in Fig. 6, the influence of the second process parameter. In Fig. 7, power is the other factor for each material, which accounts for the large variation in melting efficiency at a given travel speed. But by carefully analyzing Fig. 7, it can be seen that melting efficiency also increases with travel speed up to the theoretical maximum mentioned earlier. The large variation in melting efficiency seen in Fig. 7 illustrates the fact that parameter selection is indeed important in laser welding and that low heat input welds are not inherent to the process. If the motivation for selecting laser welding is to minimize heat input to the part, one must maximize melting efficiency. Attaining the highest melting efficiency does not depend on the level of beam irradiance or the type of material, but depends only on the levels of two selectable process para-

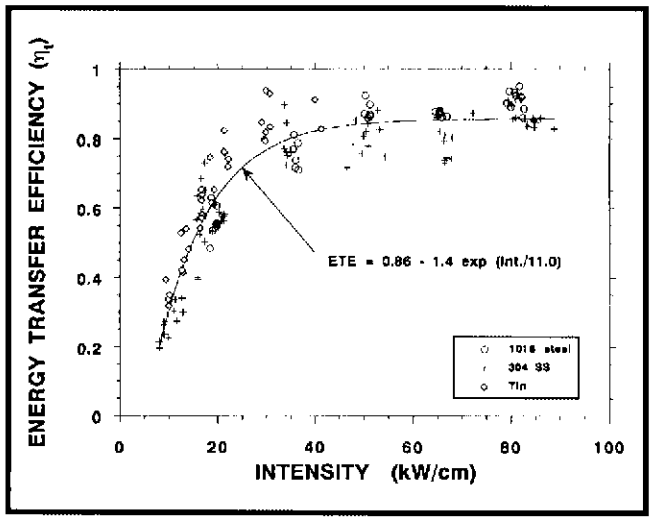

Fig. 5 — Effect of laser intensity on the measured absorption for welds on three materials.

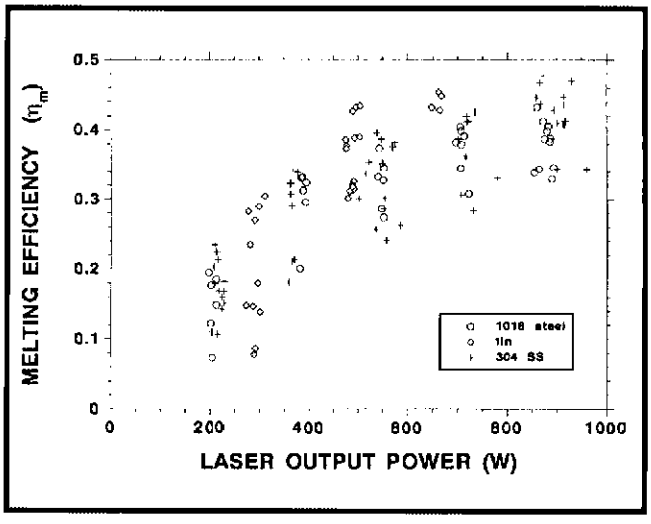

Fig. 6 — Dependence of laser melting efficiency on output power for three materials.

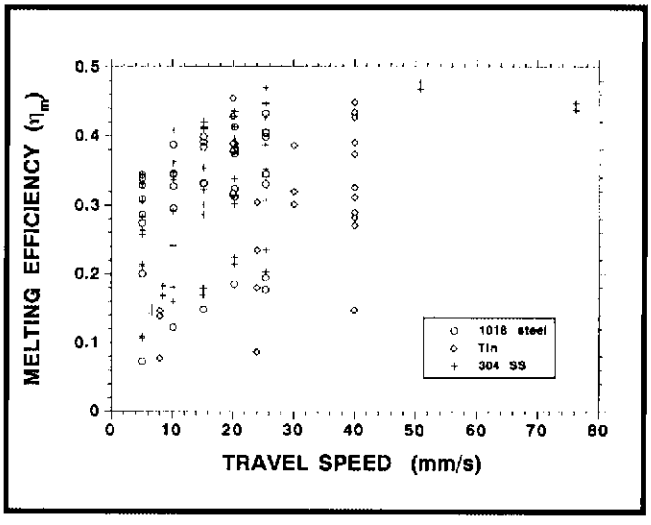

Fig. 7 — Dependence of laser melting efficiency on travel speed for three materials.

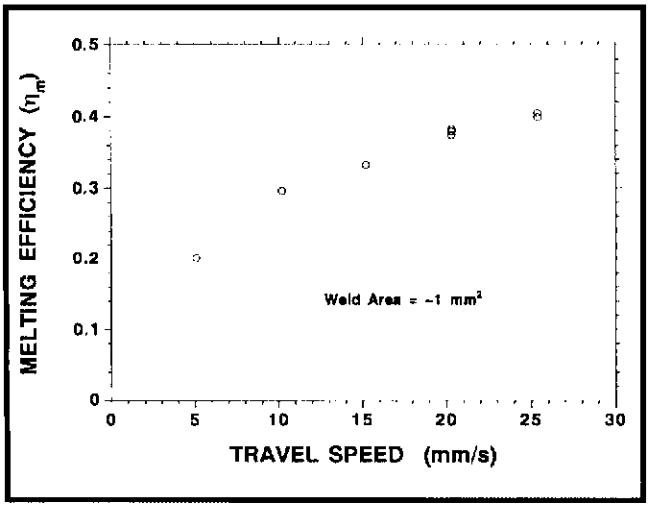

Fig. 8 — Effect of travel speed on melting efficiency for 1018 steel laser welds of equivalent size.

meters: power and travel speed.

Figure 8 shows the effect of travel speed on melting efficiency for several 1018 steel welds that have approximately the same fusion zone size. Each data point represents a particular combination of power and travel speed that results in a similar amount of melting. One can see from Fig. 8 that for the five weld schedules represented, the highest travel speeds yielded the highest melting efficiencies. As a strategy in laser weld schedule development (or for any type of continuous power fusion welding), the most direct way to increase the melting efficiency is to increase the travel speed. It is interesting to note that since laser welding is an automatic process, laser welds are typically made at very high travel speeds (V > 25 mm/s). The same is true of electron beam welding (Ref. 33). In fact, for many automatic fusion welding processes, the high travel speeds that are routinely used to increase productivity usually insure that low heat input welds will result.

It is also quite probable that for many high rate manufacturing operations the extremely fast welding travel speeds that are used may be detrimental to melting efficiency. Figure 7 indicates that for the 304 SS welds that were made at weld speeds greater than 50 mm/s, a decrease in melting efficiency occurred. Such a decrease has been predicted and explained by Berezovskii (Ref. 21). One can intuitively sense that for a given size fusion zone there is an optimum balance between travel speed and power. If the travel speed is too fast for the incident power, a larger volume of material must be heated in order to attain the temperature gradients required to achieve fusion. If the power is increased so that the fusion zone size is consistent with the fast travel speed temperature gradients, then the melting efficiency will be improved. It should be noted that lasers are often operated at maximum power and if the travel speed is too fast for the size of the fusion zone, melting efficiency will not be optimum. Clearly, if travel speed is continuously increased while maintaining constant power, a condition will be reached where no melting will occur and the melting efficiency will be zero.

Dimensional Analysis

Figures 6–8 indicate that melting efficiency is conditional on the level of two adjustable independent process parameters. While difficult to discern from these figures, it has been demonstrated in (Ref. 9) that melting efficiency additionally depends on the type of base material. In problems such as this, it is worthwhile to find a dimensionless parameter which contains all of these important factors and thereby facilitates the determination of melting efficiency from a simple mathematical relationship. An earlier attempt (Ref. 1) to do this for arc welding data found that a dimensionless parameter as given by Rykalin (Ref. 10) was not effective in correlating melting efficiency data for different materials. Subsequent attempts to correlate the present data with other dimensionless parameters were also not advantageous. It was apparent from these efforts, that the room-temperature thermal property values used in computing the dimensionless parameters were not of the correct magnitude to achieve normalization between the different materials. It was noted in the present experimental results that despite the significant difference in room-temperature thermal diffusivity between 1018 steel and 304 SS (Table 1) there was little difference in their welding behavior. It was observed that at the melting point, the thermal diffusivity of 1018 steel and 304 SS are nearly identical. When the present experimental results were compared using Rykalin's parameter but with a liquidus temperature value of thermal diffusivity, excellent correlation with melting efficiency for all of the materials studied to date was obtained. We will designate this dimensionless parameter here as: Ry, after Rykalin. We define it as follows:

$$Ry = \frac{q_i \upsilon}{\alpha^2 \delta h} \qquad (4)$$

where: q_i = net power into the workpiece; υ = travel speed; α = the thermal diffusivity at the liquidus temperature; δh = the enthalpy of melting as given in Equation 2.

The dependence of LBW melting efficiency on Ry for all three materials is shown in Fig. 9. It is apparent that this parameter results in much better experimental data correlation for melting efficiency than was the case in Figs. 6 or 7. Ry is effective in reducing the problem to one simple mathematical relationship. The form of the equation given in the figure comes from an approximate numerical solution to equations relating the dimensionless width of the weld pool to Ry as given by Christensen, *et al.* (Ref. 34). The equations given by Christensen, *et al.*, in turn were derived from the differential equation for moving point source heat flow as given by Rosenthal (Ref. 35). The constants given in the equation used in Fig. 9 were determined by curve fitting the approximate solution to the experimental data.

The implications of the excellent correlation between the experimental values of Ry and the theoretically derived relationship shown in Fig. 9 are broad. Since travel speed and power are both linear variables in Ry, one can see that increasing either one will lead to an increase in melting efficiency. Conversely, since α is in the denominator and squared, materials with greater thermal diffusivity will require much higher levels of power and travel speed in order to achieve an equivalent melting efficiency. This mathematical relationship also leads one to conclude that any material can be welded with a high melting efficiency if the power and travel speed are optimized.

The apparent data scatter about the theoretical curve in Fig. 9 is thought to be due to the uncontrolled effect of heat flow geometry. As discussed in Ref. 1, fu-

sion zone shapes that create heat flow that is more two-dimensional than three-dimensional can potentially reach a higher level of melting efficiency. Since the welds in this experiment were all made on relatively thick plates, the heat flow geometry should be three dimensional. However, ideal three-dimensional heat flow conditions, which occur when the fusion zone shape is hemispherical (*i.e.*, depth-to-width ratio = 0.5), are not often obtained in laser welding. Since the depth-to-width ratios in this experiment varied from approximately 0.5 to 1.9, Fig. 9 includes welds with heat flow that ranges from three-dimensional to near two-dimensional. The theoretical maximum melting efficiency obtainable for three-dimensional heat flow at 0.37 is moderately lower than the 0.48 predicted for two-dimensional heat flow conditions. Rykalin recognized (Ref. 10) that as the depth-to-width ratio of the fusion zone varies, the heat flow geometry will be slightly changed, and therefore, the melting efficiency will be affected.

These results suggest that LBW has an important advantage over conventional arc welding processes that cannot achieve high fusion zone depth-to-width ratios. For joint geometries that normally produce three-dimensional heat flow, LBW can achieve an enhanced melting efficiency because it results in a situation similar to two-dimensional heat flow. Since for most laser welding high depth-to-width ratio welds are obtained, one can conclude that in many instances laser welding results in moderately lower heat input for welds of equivalent size.

An important mathematical relationship using dimensionless parameters for keyhole mode laser beam welding was given by Swift-Hook and Gick (Ref. 4). The widely referenced diagram which they presented allows one to find the two efficiencies discussed above from knowledge of the material thermal properties, the laser output power, the travel speed, and the fusion zone depth and width. The diagram is given in Fig. 10 and shows the theoretical curve for a line heat source with 100% energy transfer. Also shown in Fig. 10 is the proximity of the present experimental data to the theoretical curve. The values of the dimensionless parameters given in Fig. 10 were determined using the actual net power into the part, and the measured weld penetration depth and width, (*a* and *b* respectively), for the 1018 steel and 304 SS welds made in this study. The material properties, S, a heat function in kW/m, and, α, the thermal diffusivity, used in the calculations are temperature-averaged values given in (Ref. 4). Since calorimetrically measured values of power were used to determine the dimensionless parameters, the data should lie on the theoretical curve.

The poor correlation between the present data and the line source model shown in Fig. 10 is thought to be due to the following three reasons. First, the diagram was developed for full penetration keyhole laser welding and assumes a rectangular-shaped fusion zone. Since none of the welds in this study have that shape, the model has limited applicability for these welds. Second, the use of averaged material property data likely leads to significant error, since as noted above, material property data can be very important in dimensional analysis. Third, it is questionable to use the X and Y parameters to predict weld joint penetration when they do not take into account the actual spot size of the laser beam, which was shown above to have an important effect on penetration.

However, this uncertainty in applying the diagram of Swift-Hook and Gick to laser welding does not diminish its important utility for estimating energy transfer efficiency. As was shown in Fig. 9, dimensionless parameters (Equations 3 and 4) can be used to correlate the size of a laser weld to the properties of the material, travel speed, and power required to melt that material. Figure 10 includes these same factors as well,

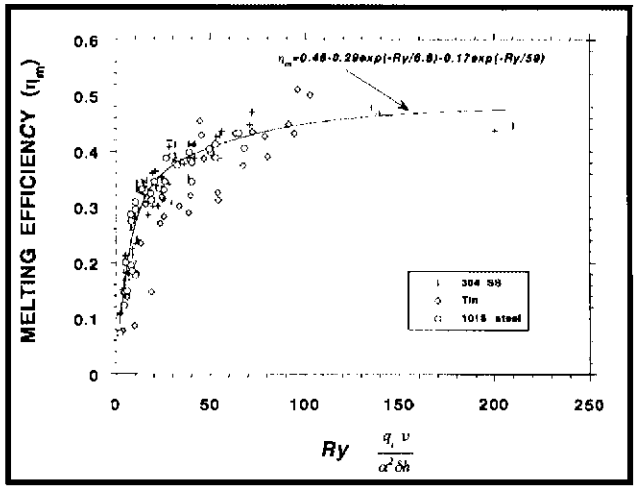

Fig. 9 — Dependence of laser melting efficiency on the dimensionless parameter, Ry, for three materials.

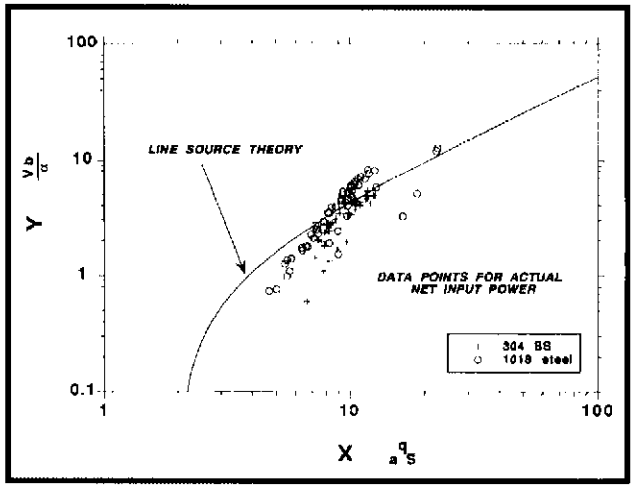

Fig. 10 — Line source model for keyhole laser beam welding from Ref. 4, datapoints are present experimental results.

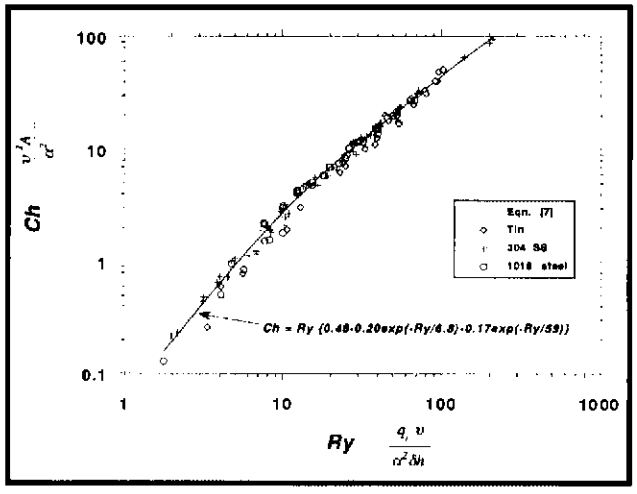

Fig. 11 — Mathematical model for continuous- power laser welding using dimensionless parameters.

but in different dimensionless groups. For the right conditions, this diagram can be used to estimate what fraction of the laser output power is actually used to produce melting, and thereby to determine the energy transfer efficiency. For a welding process that can have energy transfer to the workpiece as variable as was seen in Fig. 5, this is an important advantage. However, for most laser welding, the volume of the fusion zone cannot be accurately characterized by the weld depth and width since these values depend on factors that are not considered in this dimensionless parameter model. The same is true for predicting weld penetration with many other welding models. Since penetration is influenced by many uncontrolled factors besides power and travel speed, any penetration-based model will be necessarily less robust. However, the volume of the fusion zone is not sensitive to the same factors that affect penetration. The volume of the fusion zone should not be dependent on any other factors besides the power and the travel speed. This is apparent in the following energy balance given for welding by Hardt, *et al.* (Ref. 36):

$$q_i = q_{cond} + \delta h \frac{dV}{dt} \tag{5}$$

where q_{cond} = power conducted away from the weld; $\frac{dV}{dt}$ = rate of change of the weld pool volume

They noted that the weld pool volume is an important state variable in design of control systems for fusion welding. One can see from Equation 5 that the volume of the fusion zone is directly related to the net power into the workpiece and will change in size when the net power is changed. The conductance term depends on the thermal gradients surrounding the weld pool, and so it incorporates the melting efficiency. As the thermal gradients in the workpiece change due to variations in travel speed or power, the weld pool volume will be affected accordingly. For a constant input power, only changes in melting efficiency will alter the volume of the weld pool. Since the enthalpy of melting for liquid metals is large, the weld pool volume cannot be easily perturbed by uncontrolled effects such as weld pool chemistry or joint tolerance variability. The significance of this energy balance is that the volume of the weld pool is an easily measured and robust indicator of melting efficiency and the net heat input.

For constant speed welding, the weld cross-sectional area (A) is directly proportional to the weld pool volume and can be used to represent it. The cross-sectional areas measured in this study were found to be an important factor when applying dimensional analysis to the experimental results. A dimensionless parameter containing A that is very similar to the parameter Y in Fig. 10, was discovered to be very closely coupled with Ry. We will call this dimensionless parameter Ch, since its form was first given by Christensen, *et al.* (Ref. 34), for arc welding processes. We define it as follows:

$$Ch = \frac{v^2 A}{\alpha^2} \tag{6}$$

Unique to this definition, α again is the thermal diffusivity at the liquidus temperature.

Figure 11 illustrates the dependence of Ch on Ry for all of the laser beam welds made in this study. The extremely good agreement of the experimental results with these two dimensionless parameters is remarkable when one considers the wide variation in materials and process conditions represented here (recall the variation in Fig. 2).

The underlying mechanism responsible for the correlation of these dimensionless parameters is not yet fully understood. Dimensional analysis postulates that all physical processes can be expressed as a relationship among dimensionless parameters. It is thought that since liquidus temperature values for thermal diffusivity are required in the model, the diagram represents the heat transfer process which occurs in the weld pool at the liquid metal boundary layer located at the solid-liquid interface. At this location, the liquid metal temperature will be invariant and at the liquidus temperature. In fact, Fig. 11 is very similar to heat transfer correlations for liquid metal flow in pipes (Ref. 37), which relate the well-known Nusselt number (Nu) and Peclet number (Pe). It can be shown that Ry is similar to Nu, the convective heat transfer parameter, and Ch is similar to Pe, which is applicable for low Prandtl number fluids such as liquid metals. One should also note that in convective heat transfer applications with Nu and Pe, the thermal conductivity value used is that of the convecting fluid as is the case in Fig. 11.

The equation fit to the data in Fig. 11 is another form of the theoretically derived equation for melting efficiency given in Fig. 9. The equation in Fig. 9 has the following form:

$$\eta_m = 0.48 - 0.29 exp\left(\frac{-Ry}{6.8}\right) - 0.17 exp\left(\frac{-Ry}{59}\right) \tag{7}$$

Since melting efficiency can be defined using the same factors that are used to describe Ch and Ry, the following expression for melting efficiency can be obtained if Ch is divided by Ry:

$$\eta_m = \frac{Ch}{Ry} = \frac{v A \delta h}{q_i} \tag{8}$$

If we substitute Equation 8 into Equation 7 and rearrange terms, the following mathematical relationship between Ch and Ry is obtained.

$$Ch = Ry\left[0.48 - 0.29 exp\left(\frac{-Ry}{6.8}\right) - 0.17 exp\left(\frac{-Ry}{59}\right)\right] \tag{9}$$

As a result, Equation 9 is just another form of the equation used to correlate the data in Fig. 11. Essentially, the above equations illustrate the conjunctive relationship among the three dimensionless parameters: Ry, Ch , and η_m that is contained in the diagrams of Figs. 9 and 11. Figure 11 can be used indirectly to estimate the melting efficiency since it facilitates the determination of either Ry or Ch when the other parameter is known. After determination of the values of Ch and Ry, melting efficiency can be calculated from the ratio of Ch to Ry. In contrast, Fig. 9 more clearly illustrates the variation of melting efficiency with Ry and plainly shows the practical limitation to increasing melting efficiency beyond values of about 50 for Ry. In many circumstances, Fig. 9 can be used to estimate melting efficiency from knowledge of the weld schedule. Moreover, it is valuable because it permits the determination of melting efficiency without calculating Ch directly (which requires a cross-sectioned weld).

The usefulness of Fig. 11 is considerable and should be understood. When developing weld schedules, Equation 9 can be used to readily and accurately estimate the size of a weld for a given material, travel speed, and net power. If one is uncertain as to the magnitude of the energy transfer efficiency, it can be determined by making a weld and measuring the cross-sectional area. Only the weld area, travel speed, and material properties are needed to predict the net power from the diagram. Once the energy transfer efficiency is determined, then accurate predictions of weld size can be made for any combination of output power or travel speed, as long as the

laser intensity remains constant. The uniqueness of this dimensionless parameter model is due to Ry, since it contains the actual net power into the workpiece; the high degree of predictability of this model is likely due to the inclusion of the cross-sectional area, which is a robust indicator of weld pool heat transfer. It is important to note that since none of the factors in Ry or Ch can be considered process dependent, these parameters and the model are likely extendable to other welding processes. The thermodynamic basis of the model should permit its application to other continuous-power welding heat sources that produce fusion zones with similar heat flow geometries.

Conclusions

1) The energy transfer efficiency of continuous-wave CO_2 laser beam welding was found to increase with beam intensity from about 0.20 to 0.90, and was found to stabilize at a high value at intensities greater than 30 kW/cm. Operating in this plateau region is recommended because laser energy transfer efficiency will be insensitive to changes in laser beam intensity.

2) Energy transfer efficiency was found to be more strongly dependent on the ratio of the laser output power to the spot diameter (beam intensity) than to the ratio of the laser output power to the spot area (beam irradiance).

3) Weld pool shape and travel speed were not found to affect the energy transfer efficiency nor were especially high levels of laser power required to reach maximum energy transfer efficiency.

4) Melting efficiency for laser beam welding is no higher than the theoretical maximum of 0.48, which can be obtained with conventional arc welding processes. Melting efficiency was seen to begin to decrease at extremely high travel speeds.

5) Laser beam welding can achieve an enhanced melting efficiency in applications where three-dimensional heat flow conditions apply since the fusion zone shapes of laser welds can create heat flow that is more two-dimensional.

6) Dimensionless parameters first given by Rykalin (Ry), and Christensen (Ch), but modified by taking thermal diffusivity at its liquidus temperature, have been found to fully correlate experimental data for continuous power laser welding in a mathematical model that relates the size of a weld to the net heat input and travel speed.

7) The melting efficiency can be readily determined from this model by calculating the ratio of Ch to Ry.

8) Through application of this dimensionless parameter model, measurements of weld size can be used to estimate the energy transfer efficiency for other welding processes that exhibit two-dimensional heat flow.

Acknowledgments

The author wishes to express his sincere appreciation to Fred Hooper for his valuable assistance in operating the laser and performing the calorimetric measurements for this study. I would also like to thank Gerald Knorovsky, Michael Cieslak, and David Keicher for their insights and discussion during the completion of this work. This work was performed at Sandia National Laboratories and supported by the U.S. Dept. of Energy under contract number DE-AC04-94AL85000.

References

1. Fuerschbach, P. W. 1991. Melting efficiency in fusion welding. In *The Metal Science of Joining*. TMS: Cincinnati, Ohio, pp. 21–29.

2. Locke, E., Hoag, E., and Hella, R. 1972. Deep penetration welding with high-power CO_2 lasers. *Welding Journal* 51(5).

3. Stegman, R. L., Schriempf, J. T. 1973. Experimental studies of laser supported absorption waves with 5 ms pulses of 10.6 mm radiation. *J. Appl. Phys.* 44(8).

4. Swift-Hook, D. T., and Gick, A. F. E. 1973. Penetration welding with lasers. *Welding Journal* 52(11):492-s to 499-s.

5. Peretz, R., and Mayer, H. G. 1985. Parameter correlations for deep penetration welding with high energy focused beams. *Optics and Lasers in Engineering* 6:225–250.

6. Akhter, R., Davis, M., Dowden, J., Kapadia, P., Ley, M., and Steen, W. M. 1989. A method for calculating the fused zone of laser keyhole welds. *J. Phys. D: Appl. Phys.* 21:23–28.

7. Connor, L. P. 1987. *Welding Handbook*. Eighth ed.; American Welding Society: Vol. 1, p. 34.

8. LaRocca, A. V. 1982. Laser applications in manufacturing. *Scientific American* (March), pp. 94–103.

9. Fuerschbach, P. W., and Knorovsky, G. A. 1991. A study of melting efficiency in plasma arc and gas tungsten arc welding. *Welding Journal* 70(10):287-s to 297-s.

10. Rykalin, N. N. 1951. *Calculation of Heat Flow in Welding*, Translated by Zvi Paley and C. M. Adams Jr., Moscow.

11. Touloukian, Y. S., and Ho, C. Y., (Ed.) 1972. *Thermophysical Properties of Matter*. Plenum Press: New York.

12. Pehlke, R. D., Jeyarajan, A., and Wada, H. 1982. *Summary of Thermal Properties for Casting Alloys and Mold Materials*, National Science Foundation, NSF/MEA-82028.

13. Leibowitz, L. 1976. *Properties for LMFBR Safety Analysis*, Argonne National Labs, ANL-CEN-RSD-76-1.

14. Kelley, K. K. 1960. *Contributions to the Data on Theoretical Metallurgy*, U.S. Bureau of Mines, Washington, D.C., Bulletin 584.

15. Myers, P. S., Uyehara, O. A., and Borman, G. L. 1967. *Fundamentals of Heat Flow in Welding*, Welding Research Council, 123.

16. Benzinger, T. H., and Kitzinger, C. 1949. Direct calorimetry by means of the gradient principle. *The Review of Scientific Instruments* 20(12):849–860.

17. Giedt, W. H., Tallerico, L. N., and Fuerschbach, P. W. 1989. GTA welding efficiency: calorimetric and temperature field measurements. *Welding Journal* 68(1):28-s to 32-s.

18. Essien, M., and Fuerschbach, P. W. 1993. Beam Quality of a Materials Processing CO_2 Laser. Accepted for publication in *Welding Journal*.

19. Fuerschbach, P. W., and Essien, M. 1993. Beam-quality measurements for materials processing lasers and the proposed ISO standard. In *ICALEO*. LIA, Orlando, Fla., pp. 312–322.

20. Brandon, E. D. 1992. Characterization of focusing lenses used for CO_2 laser beam welding. *Welding Journal* 71(6):55–63.

21. Berezovskii. 1979. The thermal efficiency of the process of penetrating metals with a welding arc at the surface. *Automatic Welding* 10:18–21.

22. ANSI/ASME. 1986. *Measurement Uncertainty*, ANSI/ASME PTC 19.1-1985, 1986.

23. Maher, W. E., and Hall, R. B. 1978. Experimental thermal coupling of laser beams. *J. Appl. Phys.* 49(4):2254–2261.

24. Huntington, C. A., and Eagar, T. W. 1983. Laser welding of aluminum and aluminum alloys. *Welding Journal* 62(4):105-s to 107-s.

25. Kim, T. H., Albright, C. E., and Chiang, S. 1990. The energy transfer efficiency in laser welding process. *Journal of Laser Applications* (Jan/Feb):23–28.

26. Bramson, M. A. 1968. *Infrared Radiation, A Handbook for Applications*; Plenum Press, New York, p.133.

27. Arata, Y. 1986. *Plasma, Electron and Laser Beam Technology*. ASM, Materials Park, Ohio, p. 237.

28. Mallory, L. C., Orr, R. F., and Wells, W. 1988. The effect of anodizing on laser welding of aluminum. In *Third Symposium on Laser Materials Processing*. TMS, Chicago, Illinois, pp. 123–134.

29. Beyer, E., Bakowsky, L., Loosen, P., Poprawe, R., and Herziger, G. 1983. Development and optical absorption properties of a laser induced plasma during CO_2 laser processing. *SPIE*, pp. 75–80.

30. Beyer, E., Behler, K., and Herziger, G. 1988. Influence of laser beam polarization in welding. *Lasers in Manufacturing—5*.

31. Mazumder, J. 1981. Laser welding: state of the art review. *Lasers in Metallurgy*. The Metallurgical Society of AIME, Chicago, Illinois.

32. Hoult, A., and Dijk, M. V. 1988. High power Nd:YAG laser welding. *Industrial Laser Review* (September).

33. Elmer, J. W., Giedt, W. H., and Eagar, T. W. 1990. The transition from shallow to deep penetration during electron beam welding. *Welding Journal* 69(5):167-s to 176-s.

34. Christensen, N., Davies, V. L., and Gjermundsen, K. 1965. Distribution of tem-

peratures in arc welding. *British Welding Journal* 12(12):54–75.

35. Rosenthal, D. 1946. The theory of moving sources of heat and its application to metal treatments. *Transactions of the ASME* (November):849–866.

36. Hardt, D. E., Garlow, D. A., and Weinert, J. B. 1985. A model of full penetration arc-welding for control system design. *ASME Journal of Dynamic Systems, Measurement, and Control* 107(3):40–46.

37. Eckert, E. R. G., and Drake, R. M. 1972. *Analysis of Heat and Mass Transfer*, McGraw-Hill, New York.

Appendix

Table 3 of experimental uncertainty is applicable to one specific weld made on 1018 steel. This weld was chosen as a nominal value because it is representative of many of the measurements made. For each of the other welds in this study, the reported values of measurement uncertainty may be higher or lower than the values reported in this table. The terminology and calculations used to produce the above table are taken from the ANSI/ASME *Standard on Measurement Uncertainty* issued in 1986 (Ref. 22). The bias and precision limits given are for a 95% confidence level. The overall uncertainty for each parameter is calculated using the root-sum-square method. A brief discussion of the significance of the uncertainty for each parameter follows:

Output Power — The bias error is greater than the precision error for the laser power measurements because the repeatability of the power probe measurement and the stability of the laser power are both better than the power probe accuracy as stated by the manufacturer.

Net Power — The net power measured by the calorimeter has lower bias error than precision error because it was calibrated for the experiment. The precision error represents the variation from weld to weld for similar conditions.

Weld Area — Calibration of the planimeter essentially eliminates the bias error. The precision error is due to the variation in weld cross-sectional area among the four metallographic sections made.

Table 3 — Experimental Uncertainty Applicable to a Specific Weld Made on 1018 Steel

Parameter	Nominal Value	Bias Limit	Precision Limit	Overall Uncertainty	Percent Uncertainty
Output Power (watts)	541	±23.6	±12.3	±26.6	±4.9%
Net Power (watts)	472	±6.57	±32.4	±33.0	±7.0%
Weld Area (mm^2)	0.989	±0.0002	±0.113	±0.113	±11.4%
Spot Diameter (mm)	0.118	unknown	±0.009	±0.009	±7.63%
Irradiance (MW/cm^2)	4.97	±0.22	±0.76	±0.791	±15.9%
Intensity (kW/cm)	50.1	±2.00	±3.65	±4.16	±8.31%
η_m	0.332	±0.0056	±0.044	±0.044	±13.3%
η_i	0.872	±0.040	±0.063	±0.746	±8.55%
Ry	22.8	±2.57	±1.56	±3.01	±13.2%
Ch	7.55	±0.757	±0.747	±1.06	±14.1%

Spot Diameter — No suitable estimate of the bias error for the Prometec instrument is available. The precision error includes the deviation from the laser beam propagation equation as well as the repeatability of the Prometec measurements.

Irradiance — The bias error is smaller than its true value since the bias error of the spot diameter is unknown. The precision error alone is significant however, especially since the spot diameter is a squared term in irradiance.

Intensity — As for irradiance, the bias error is smaller than its true value since the bias error of the spot diameter is unknown. Since the spot diameter is not squared, the overall uncertainty for intensity is lower than for irradiance.

Melting efficiency (η_m) — The bias error is primarily affected by the net power bias. The enthalpy of melting bias error was arbitrarily chosen to be 5% and was relatively insignificant in comparison. The precision error component that is most significant is the weld area.

Energy transfer efficiency (η_i) — The bias error is primarily influenced by the bias of the output power measurement. The precision error is primarily affected by the precision of the net power measurement.

Ry — Since the thermal diffusivity is a squared term in the calculation of Ry, it has a strong effect on the bias error. Because thermal diffusivity measurements for liquid metals are very rare, it is not surprising to find that estimates of accuracy are not given. The bias limit for thermal diffusivity was arbitrarily chosen to be ±5.0%. If the true bias error is greater than this number, the calculations of Ry will have a greater uncertainty. The precision error for Ry is primarily influenced by the bias error for net power.

Ch — As was the case for Ry, the bias error for Ch is primarily influenced by the uncertainty in thermal diffusivity. The precision error is most affected by the precision error in the area measurements.